

1 **Supplement for**
2 **“Theoretical Framework for Measuring Cloud Effective**
3 **Supersaturation Fluctuations with an Advanced Optical System”**

4 Ye Kuang¹, Jiangchuan Tao¹, Hanbin Xu², Li Liu³, Pengfei Liu⁴, Wanyun Xu⁵, Weiqi Xu⁶, Yele Sun⁶,
5 Chunsheng Zhao⁷

6 ¹ Institute for Environmental and Climate Research, College of Environment and Climate, Jinan
7 University, Guangzhou, Guangdong, China

8 ² Experimental Teaching Center, Sun Yat-Sen University, Guangzhou, China

9 ³ Key Laboratory of Regional Numerical Weather Prediction, Institute of Tropical and Marine
10 Meteorology, China Meteorological Administration, Guangzhou, China.

11 ⁴ School of Earth and Atmospheric Sciences, Georgia Institute of Technology, Atlanta, GA, USA

12 ⁵ State Key Laboratory of Severe Weather, Key Laboratory for Atmospheric Chemistry, Institute of
13 Atmospheric Composition, Chinese Academy of Meteorological Sciences, Beijing, China

14 ⁶ State Key Laboratory of Atmospheric Boundary Layer Physics and Atmospheric Chemistry, Institute
15 of Atmospheric Physics, Chinese Academy of Sciences, Beijing, China.

16 ⁷ Department of Atmospheric and Oceanic Sciences, School of Physics, Peking University, Beijing,
17 China.

18

19

20 Correspondence: Ye Kuang (kuangye@jnu.edu.cn)

21

22

23 **Contents of this file**

24 **Section S1:** The reason we choose PM1 of total aerosol populations as the reference

25 **Section S2:** Simulation details of the relationships between D_a and f_{sp}

26 **Section S3:** Other supplementary Figures, Figure S1-2

27 **1. The reason we choose PM₁ of total aerosol populations as the reference**

28 In clouds, part aerosol activates into cloud droplets, and the rest of them remain as interstitial
29 aerosols. Therefore, the scatterings of total aerosol populations in dry state $\sigma_{sp,all}(\lambda)$ can be expressed:

30
$$\sigma_{sp,all}(\lambda) = \sigma_{sp,inter}(\lambda) + \sigma_{sp,act}(\lambda) \quad (1)$$

31 Where $\sigma_{sp,inter}(\lambda)$ and $\sigma_{sp,inter}(\lambda)$ represent scatterings of interstitial aerosols and activated aerosols
32 in dry state, and λ is the optical wavelength.

33 If using 1 μm as the threshold of activated aerosols, $\sigma_{sp,inter}(\lambda)$ can be expressed as:

34
$$\sigma_{sp,inter}(\lambda) = \sigma_{sp,inter,PM_1}(\lambda) \quad (2)$$

35 Where $\sigma_{sp,inter,PM_1}(\lambda)$ represents scatterings of interstitial aerosols that are PM₁ in dry state, and
36 $\sigma_{sp,inter,PM_{1-2.5}}(\lambda)$ represents scatterings interstitial aerosols that are in the aerodynamic diameter
37 range of 1-2.5 μm . And the $\sigma_{sp,act}(\lambda)$ can be expressed as:

38
$$\sigma_{sp,act}(\lambda) = \sigma_{sp,act,PM_1}(\lambda) + \sigma_{sp,act,PM_{1-2.5}}(\lambda) + \sigma_{sp,act,PM_{>2.5}}(\lambda) \quad (3)$$

39 Where $\sigma_{sp,act,PM_1}(\lambda)$ represents scatterings of activated aerosols that are PM₁ in dry state,
40 $\sigma_{sp,act,PM_{1-2.5}}(\lambda)$ represents scatterings of activated aerosols that are in the aerodynamic diameter
41 range of 1-2.5 μm and $\sigma_{sp,act,PM_{>2.5}}(\lambda)$ represents scatterings of activated aerosols that are in the
42 aerodynamic diameter range of >2.5 μm . Therefore, $\sigma_{sp,all}(\lambda)$ can be expressed as:

43
$$\sigma_{sp,all}(\lambda) = \sigma_{sp,inter,PM_1}(\lambda) + \sigma_{sp,act,PM_1}(\lambda) + \sigma_{sp,act,PM_{1-2.5}}(\lambda) + \sigma_{sp,act,PM_{>2.5}}(\lambda) \quad (4)$$

44 If a PM₁ impactor were not used after water vapor evaporated for the TSP inlet measurements. Then
45 the ratio $f_{sp} = \sigma_{sp,inter}(\lambda)/\sigma_{sp,all}(\lambda)$ lower than 1 could corresponding to two scenarios: (1) part of
46 submicron aerosols have activated with $\sigma_{sp,act,PM_{>1}}(\lambda)$ are negligible; (2) no aerosols are activated
47 with $\sigma_{sp,act,PM_{>1}}(\lambda)$ are not negligible. That means, we could observe f_{sp} lower than 1 under both
48 subsaturated conditions and supersaturated conditions, and this would obscure the D_a retrievals in
49 cloud conditions, especially at lower supersaturations, when D_a is higher and $\sigma_{sp,inter}(\lambda)$ itself is
50 relatively small. However, if a PM1 impactor is placed downstream of the inlet and upstream of the
51 two nephelometers (or other optical instruments), the observed f_{sp} can be expressed:

52
$$f_{sp} = \sigma_{sp,inter,PM_1}(\lambda)/(\sigma_{sp,inter,PM_1}(\lambda) + \sigma_{sp,act,PM_1}(\lambda)) \quad (5)$$

53 f_{sp} be lower than 1 could only be caused by activation of submicron aerosols, therefore, facilitate the
54 accurate retrieval of D_a .

55 If using 2.5 μm as the threshold of activated aerosols, $\sigma_{sp,inter}(\lambda)$ can be expressed as:

$$56 \quad \sigma_{sp,inter}(\lambda) = \sigma_{sp,inter,PM_1}(\lambda) + \sigma_{sp,inter,PM_{1-2.5}}(\lambda) \quad (6)$$

57 the $\sigma_{sp,act}(\lambda)$ can be expressed as:

$$58 \quad \sigma_{sp,act}(\lambda) = \sigma_{sp,act,PM_1}(\lambda) + \sigma_{sp,act,PM_{1-2.5}}(\lambda) + \sigma_{sp,act,PM_{>2.5}}(\lambda) \quad (7)$$

59 A $PM_{2.5}$ impactor downstream of TSP inlet after water evaporates would eliminate the influences of
60 $\sigma_{sp,act,PM_{>2.5}}(\lambda)$. However, as demonstrated in Kuang et al. (2018), the $\sigma_{sp,all}(\lambda)$ are not sensitive to
61 changes in super-micron aerosols therefore it would be better if only submicron aerosols are included
62 in observing the scattering fractions of interstitial aerosols and benefits for accurate retrieval of D_a .
63 Therefore, no matter using 1 or 2.5 μm as the threshold, the PM_1 impactor are suggested downstream
64 of the inlet system after heating.

65 As mentioned, In the concept design of Sect.4 of the manuscript, the interior PM_1 impactor was
66 placed downstream of the inlet system where RH of sample air was heated down to 70%. RH down to
67 70% is to make sure selected aerosols using the PM_1 impactor are very close to aerosols populations
68 of PM_1 in dry state based on the investigates of impacts of aerosol hygroscopic growth on cut-off size
69 shift of impactors (Xu et al., 2024).

70

71 **2. Simulation details of the relationships between D_a and f_{sp}**

72 The particle number size distributions (PNSDs) in dry state, which range from about 10 nm to 10
73 μm , were jointly measured by a Twin Differential Mobility Particle Sizer (TDMPS, Leibniz-Institute
74 for Tropospheric Research, Germany; Birmili et al. (1999)) or a scanning mobility particle size
75 spectrometer (SMPS) and an Aerodynamic Particle Sizer (APS, TSI Inc., Model 3321) in six field
76 campaigns conducted on the North China Plain which are detailed in Kuang et al. (2018). The mass
77 concentrations of black carbon (BC) were measured using a Multi-Angle Absorption Photometer
78 (MAAP Model 5012, Thermo, Inc., Waltham, MA USA) or an aethalometer (AE33) (Drinovec et al.,
79 2015) in these field campaigns. For each paired PNSD and BC mass concentration, the size distribution
80 of PM_1 (and the penetration curve shape from Gussman et al. (2002) was also included for considering
81 the non-ideality cutoff of the impactor, and assuming aerosol density of 1.6 g/cm^3 for converting
82 aerodynamic diameter to mobility diameter) :

$$83 \quad \text{PNSD } (D_p)_{PM_1} = \text{PNSD } (D_p) \times R(D_p) \quad (8)$$

84 Where $R(D_p)$ is the penetration ratio of aerosols as a function of particle diameter D_p of the PM_{10}
85 impactor.

86 One hundred size-resolved activation curves are produced for each PNSD $(D_p)_{PM_{10}}$ using the following
87 formula:

$$88 \quad AR(D_p) = \frac{MAF}{2} \left(1 + \operatorname{erf} \left(\frac{D_p - D_a}{\sqrt{2\pi}\sigma} \right) \right) \quad (9)$$

89 Where $AR(D_p)$ was the size-resolved activation ratios, MAF is the maximum activation fraction and
90 D_a is critical activation diameter, σ is associated with the slope of the curve near D_a . This formula was
91 previously proposed by (Rose et al., 2008) to fit the AR measurements and widely used in AR
92 parameterizations (Tao et al., 2018). The random ranges of MAF, D_a and σ are 0.6-1, 80-800 nm, and
93 10-100 to produced enough types of activation curves for each PNSD $(D_p)_{PM_{10}}$.

94 Therefore, the PNSD of interstitial aerosols can be calculated as the following:

$$95 \quad \text{PNSD } (D_p)_{PM_{10},inter} = \text{PNSD } (D_p)_{PM_{10}} \times (1 - AR(D_p))$$

96 Therefore, the $\sigma_{sp,PM_{10},all}(dry, \lambda)$ and $\sigma_{sp,PM_{10},inter}(dry, \lambda)$ at wavelengths of 450 nm, 525 nm and
97 636 nm for all PNSD $(D_p)_{PM_{10},inter}$ and PNSD $(D_p)_{PM_{10}}$ can be calculated using the Mie theory
98 calculations with the BC mass are distributed based on $AR(D_p)$ and the shape of black carbon mass
99 size distributions are consistent with the one used in simulations of Kuang et al. (2017) assuming
100 fractions of BC mass that are externally mixed is 0.5. Details about the Mie theory calculations can
101 also be found in Kuang et al. (2017). With these configurations, more than million pairs of f_{sp} and D_a
102 are simulated.

103

104

105

106

107

108

109

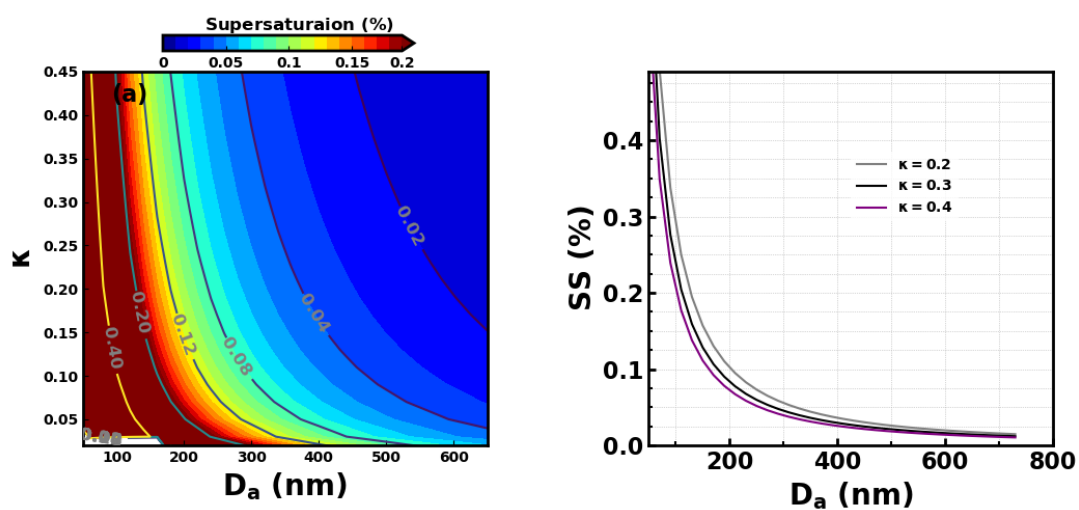
110

111

112

113 3. Other Supplementary Figures

114



115 **Figure S1.** (a) Supersaturation (SS) variations under different D_a and κ scenarios; (b) The variations
116 SS as a function of D_a for constant κ values of 0.2,0.3,0.4.

117

118

119

120

121

122

123

124

125

126

127

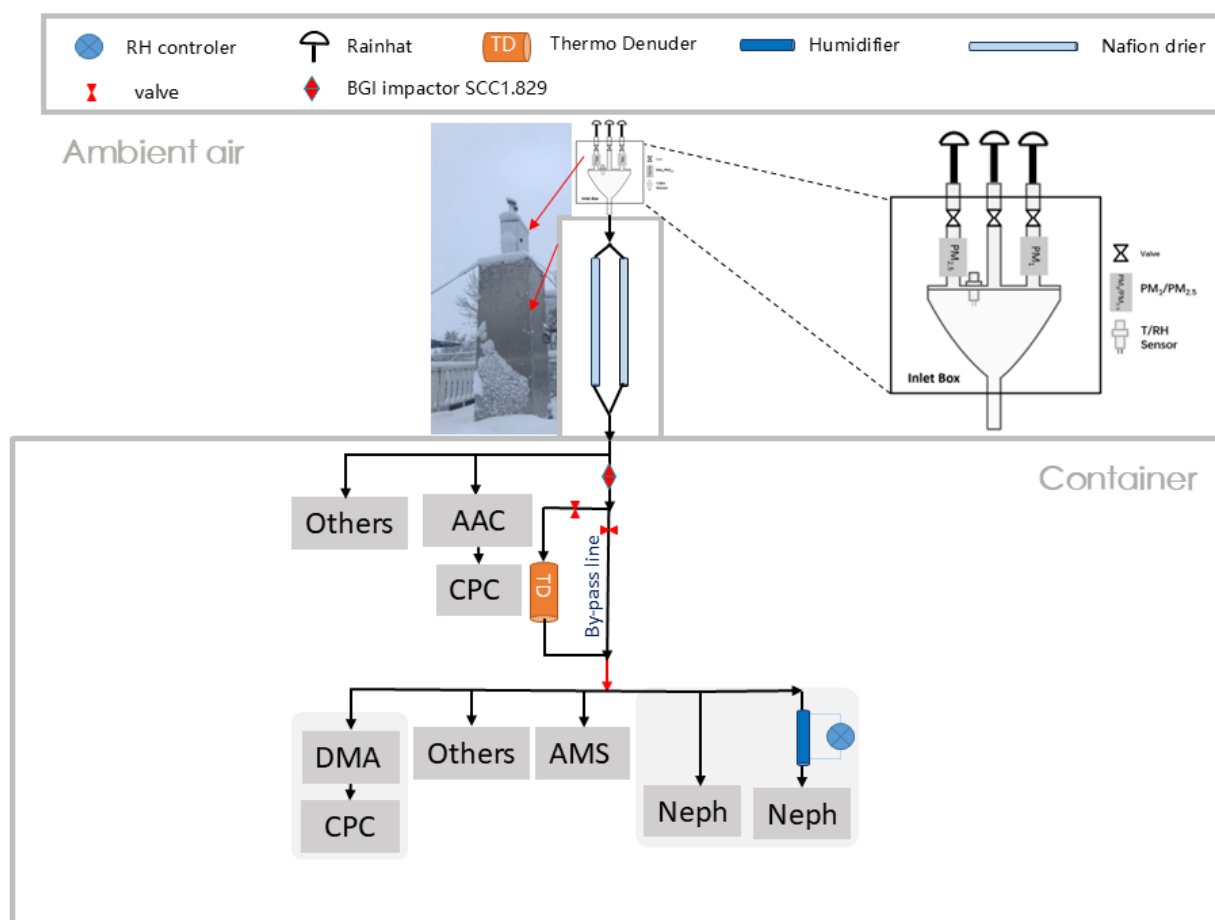
128

129

130

131

132



133 **Figure S2.** Schematic of instrument setup during the AQ-SOFAR campaign, with aerosol size
 134 distributions are measured using Aerodynamic Aerosol Classifier (AAC) and Differential Mobility
 135 Analyzer (DMA) coupled with Condensation Particle Counters (CPC, TSI 3076 and 3075), and Neph
 136 represents nephelometer.

137

138

139

140

141 **References:**

142 Drinovec, L., Močnik, G., Zotter, P., Prévôt, A. S. H., Ruckstuhl, C., Coz, E., Rupakheti, M., Sciare,
 143 J., Müller, T., Wiedensohler, A., and Hansen, A. D. A.: The "dual-spot" Aethalometer: an improved
 144 measurement of aerosol black carbon with real-time loading compensation, Atmospheric
 145 Measurement Techniques, 8, 1965-1979, 10.5194/amt-8-1965-2015, 2015.

146 Gussman, R. A., Kenny, L. C., Labickas, M., and Norton, P.: Design, Calibration, and Field Test of a
 147 Cyclone for PM 1 Ambient Air Sampling, Aerosol Science and Technology, 36, 361-365,
 148 10.1080/027868202753504461, 2002.

149 Kuang, Y., Zhao, C., Tao, J., Bian, Y., Ma, N., and Zhao, G.: A novel method for deriving the aerosol
150 hygroscopicity parameter based only on measurements from a humidified nephelometer system,
151 *Atmos. Chem. Phys.*, 17, 6651-6662, 10.5194/acp-17-6651-2017, 2017.

152 Kuang, Y., Zhao, C. S., Zhao, G., Tao, J. C., Xu, W., Ma, N., and Bian, Y. X.: A novel method for
153 calculating ambient aerosol liquid water content based on measurements of a humidified nephelometer
154 system, *Atmospheric Measurement Techniques*, 11, 2967-2982, 10.5194/amt-11-2967-2018, 2018.

155 Rose, D., Gunthe, S. S., Mikhailov, E., Frank, G. P., Dusek, U., Andreae, M. O., and Pöschl, U.:
156 Calibration and measurement uncertainties of a continuous-flow cloud condensation nuclei counter
157 (DMT-CCNC): CCN activation of ammonium sulfate and sodium chloride aerosol particles in theory
158 and experiment, *Atmos. Chem. Phys.*, 8, 1153-1179, 10.5194/acp-8-1153-2008, 2008.

159 Tao, J., Zhao, C., Ma, N., and Kuang, Y.: Consistency and applicability of parameterization schemes
160 for the size-resolved aerosol activation ratio based on field measurements in the North China Plain,
161 *Atmospheric Environment*, 173, 316-324, <https://doi.org/10.1016/j.atmosenv.2017.11.021>, 2018.

162 Xu, W., Kuang, Y., Xu, W., Zhang, Z., Luo, B., Zhang, X., Tao, J., Qiao, H., Liu, L., and Sun, Y.:
163 Hygroscopic Growth and Activation Changed Submicron Aerosol Composition and Properties in
164 North China Plain, *EGUsphere*, 2024, 1-20, 10.5194/egusphere-2024-998, 2024.

165